ACS Photonics

Article

pubs.acs.org/journal/apchd5

Near-Infrared Selective and Angle-Independent Backscattering from Magnetite Nanoparticle-Decorated Diatom Frustules

Haiyan Li,[†] Bin Jiang,[‡] Xiulun Yang,[§] Micah Eastman,[†] Yuming Liu,[∥] Linhui Wang,[§] Jeremy Campbell,[⊥] Lester Lampert,[†] Ruikang K. Wang,[∥] Gregory L. Rorrer,[⊥] and Jun Jiao*,[†]

[†]Department of Mechanical & Materials Engineering, Portland State University, Portland, Oregon 97201, United States

[‡]Fariborz Maseeh Department of Mathematics and Statistics, Portland State University, Portland, Oregon 97201, United States

[§]Department of Optics, Shandong University, Jinan 250100, China

[∥]Department of Bioengineering, University of Washington, Seattle, Washington 98195, United States

[⊥]School of Chemical, Biological, and Environmental Engineering, Oregon State University, Corvallis, Oregon 97331, United States

Supporting Information

ABSTRACT: Periodic heterogeneous structures exhibit color with brilliance through constructive interference of electromagnetic waves in accordance with Bragg's law. However, the wavelength of diffracted light is strictly angle-dependent, and such periodic structures generate only iridescent color. Here we report that periodically porous, microellipsoidal shells of diatom *Pinnularia* sp. wavelength-selectively backscatter light at arbitrary incidence. The biosilica frustules could be approximated as many polygonal faces of two-dimensional photonic crystal slabs. Furthermore, surface decoration of the frustule with magnetite nanoparticles produced photonic band gaps in the near-infrared. Magnetite nanoparticle-decorated frustules behave as angle-independent near-infrared reflectors and near-infrared contrast agents in optical coherence tomography.

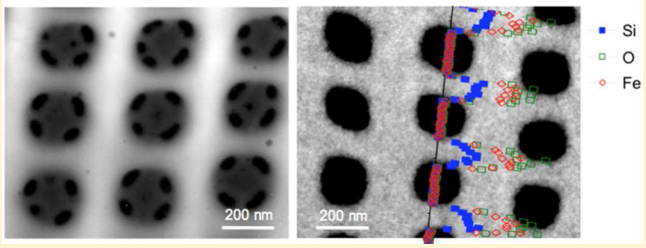

KEYWORDS: *diatom frustules, 2-D photonic crystal, near-infrared, angle-independent, optical coherence tomography*

Throughout evolution, natural species have exploited different kinds of photonic structures for strategic manipulation of light,[1,2] as can be observed in butterfly wings, bird feathers, and insect eyes. Diatoms, a prolific class of unicellular photosynthetic algae, have biomineralized biosilica cell walls, known as frustules, with micro- or nanoscale periodicity.[3,4] The frustule mechanically protects the cell and provides access to the external environment.[5] Interestingly, their chloroplasts adjust their proximity to the cell wall in response to the intensity of incident light.[6] This hints at the optical function of the patterned biosilica valves for efficient photosynthesis. The exquisite and periodic submicrometer-scale pore array of diatom frustules shares the same structural characteristics as a 2-D photonic crystal.[7,8] The photonic band structure of diatom *Coscinodiscus granii* frustules implies that transverse electrical (TE) mode resonances exist in the visible range.[9] Furthermore, some electroluminescence (EL) emissions from germanium-doped frustules of diatom *Pinnularia* sp. coincide with their calculated TE mode resonances.[10] However, a significant feature—shell curvature—distinguishes the frustule from a 2-D photonic crystal.

To discover the role of shell curvature in optical phenomena, we investigated ellipsoidal frustules of diatom *Pinnularia* sp., which consist of two biosilica valves, epitheca and hypotheca, with identical periodicity. The scanning electron microscopy (SEM) and transmission electron microscopy (TEM) images of diatom frustules are shown in Figure 1a and b. SEM analysis reveals that the broken part of frustule adhered to a Si substrate (Figure 1c), although most of diatom frustules kept ellipsoidal shapes (Figure 1d). To observe the reflection variations between the planar broken frustule and the unbroken ellipsoidal frustule, we dispersed diatom frustules onto a glass substrate. The planar areas of the frustule exhibited little reflection at normal incidence (Figure 1e). This optical phenomenon is very similar to that of a typical planar 2-D photonic crystal. Remarkably, we observed an increase of reflection from the curved portion of the valve that was not pinned to the glass substrate (Figure 1f) and efficient reflection from the unbroken frustule (Figure 1g).

To numerically estimate the reflectivity difference between the planar valve and intact frustule, each frustule was treated identically by neglecting the lattice symmetry fluctuation induced by successive generations of diatoms. This approximation was based on our SEM observations of 20 frustules, each showing less than 10% variation in lattice symmetry. The porous biosilica shell was approximated as having a lattice constant of 325 nm, a shell thickness of 50 nm (Figure S2 and S3), and a pore diameter of 200 nm. To simplify the simulation, the intact frustule was approximated as a rolled up 2-D porous

Received: November 15, 2013
Published: May 15, 2014

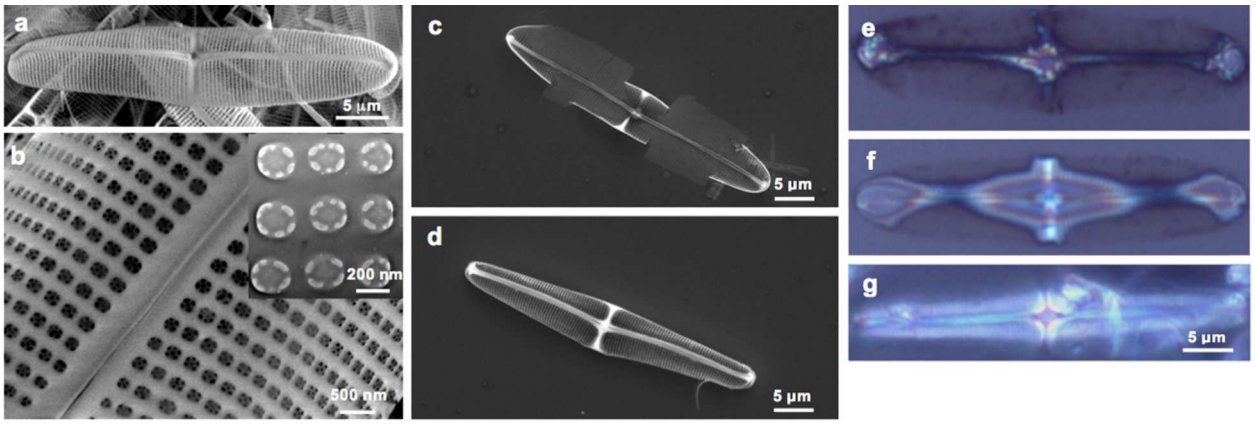

Figure 1. Diatom frustule is an efficient light reflector. (a) SEM image of stacked diatom *Pinnularia* sp. frustules. (b) SEM and TEM images (inset) of the ordered pore structure present on the surface of the diatom frustule. (c) Representative SEM image of a diatom frustule adhered to the surface of the substrate (planar frustule shell), nearly eliminating the majority of curvature typically observed for *Pinnularia* sp. frustules as seen in (d) a typical, isolated *Pinnularia* sp. diatom frustule. The planar shells from broken frustules retain their ordered pore structures (Figure S1). (e, f, and g) Optical images of planar frustule shell, curved frustule shell, and an unbroken frustule on a glass microscope slide illuminated by a halogen lamp, respectively.

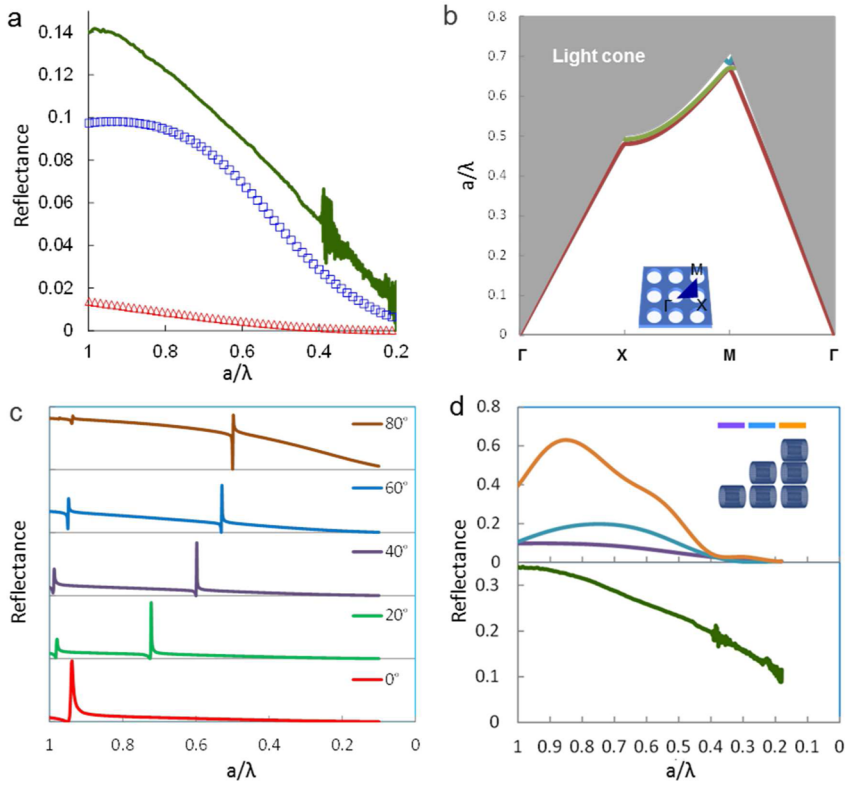

Figure 2. Frustules efficiently reflected violet light at arbitrary incidence. (a) Calculated reflection spectra of the planar frustule shell (red triangle) and the intact frustule (blue square), measured reflection spectrum of a film consisting of nearly monodispersed frustules on a glass substrate (solid green line). (b) TE-like mode photonic band structure of frustules in air. Inset of b is the approximated square lattice of air pores in biosilica. (c) Calculated angle-resolved reflection spectra of the 2D photonic crystal slab approximated from the frustules. (d) Top, FDTD-calculated reflectance spectra of mono- (purple), double- (blue), and triple- (orange) layered frustule films; bottom, measured spectra of stacked (approximately 2 or 3 layers) frustules.

silica (n = 1.48) photonic crystal slab to form a hollow cylinder, rather than a hollow ellipsoid, which could lead to local anomalies of the pore pattern at the boundary. The reflectivity of the intact frustule in air was evaluated using a finite-difference time-domain (FDTD) method.[11] The cylindrical structure exhibited around 10% reflectivity in the violet light range, a 7-fold increase in comparison to that of the planar slab (Figure 2a). This suggests that rolling up a periodic 2-D photonic crystal to form a hollow cylinder could increase the photonic structure's reflectivity. Similar to the cylindrical structure, an ellipsoid-like frustule could lead to an efficient reflection of light. In order to experimentally validate the simulated results, we collected an optical spectrum from a quasi-monolayer frustule film (thereby circumventing the

dx.doi.org/10.1021/ph4001185 | ACS Photonics 2014, 1, 477−482

difficulties inherent in collecting the optical spectrum from a single frustule). Considering the reflectivity loss (1−2%, the UV range being the exception) introduced by our geometric simplification of the frustule as a cylinder rather than an ellipsoid, the simulated reflection had a reasonable accordance with our measured spectrum.

We also approximated the intact frustule as an ellipsoidal-like polyhedron composed of 2-D photonic crystal slabs. Under this assumption, the reflectivity of the ellipsoidal-like frustule should be similar to that of the approximated polyhedron. Simulating the frustule as a hollow cylinder would estimate the reflectivity of a frustule in different wavelengths. Although the simulation of a "slab" of hollow cylinders may not predict the reflectivity of a whole frustule, it reveals the correlation between the wavelength-selective reflectivity and the ordered pore structures of frustules. The band structure of the polygonal face was determined by three-dimensional (3-D) calculations.[12] Radiation modes were shaded in the light cone region. Among guided modes, no photonic band gap (PBG) was found (Figure 2b). Since no PBG exists from the near-infrared (NIR) to the visible range, light is allowed from in-plane propagation; thus no reflective peak is observed in those regions. Next, we calculated their angular-dependent reflectance spectra in the Γ−X direction with TE polarization using a scattering matrix method.[13] All simulated spectra show a gradual reduction of the reflection intensity from the ultraviolet to visible range (Figure 2c). Abrupt local dips in these spectra originate from light coupling to in-plane photonic band modes. With greater curvature, the 2D photonic slab encounters incident light at a greater angle; hence with greater angles of incidence there are greater reflectivities. This explains the reason that the shell curvature improves reflectance of the 2-D photonic crystal slab under normal incidence.

Furthermore, this curvature allows 2-D photonic crystal slabs to form a long-range isotropic structure, such as the quasi-ellipsoidal frustule. The long-range isotropic alignment of short-range ordered nanostructures has been revealed as a mechanism for noniridescent structural coloration of avians.[14] Similarly, the assumed polygonal faces of the frustule possess angle-resolved reflection. If viewing the whole frustule as a single pixel, it almost equally reflects the light at arbitrary incidence. Therefore, the ellipsoidal frustules reflect light at arbitrary incidence without position adjustment. This is in agreement with the observation that diatoms are less sensitive to ultraviolet-B radiation than phytoplankton without external patterned silica skeletons.[15] We further calculated the reflectivity of stacked frustules, in which the thickness of each layer is around 5 μm and there is no significant space separation between the layers. Both our calculations and measurements indicate that stacked frustules have stronger light reflection than the film consisting of monodispersed frustules in similar wavelength ranges (Figure 2d). This thickness effect of the frustule film is comparable to the reflectance enhancements of 3-D photonic crystals induced by increasing their thickness.[16]

Increasing the refractive index contrast of frustule pore structures could create PBG-associated reflection.[17] In an effort to increase the refractive index of the diatom frustules, we decorated the biosilica frustules with magnetite (n = 2.42) through a solvothermal reaction, which is capable of growing uniform magnetite nanoparticles (NPs) at 185 °C (Figure S4). Since this is a gentle fabrication process, it enables the as-fabricated magnetite NP-decorated frustules to maintain the original shape of the bare frustules (Figure S5), except for the destruction of the fragile silica pore lining and a slight reduction of the pore size (Figure 3a and b). The elemental (Fe, O, and

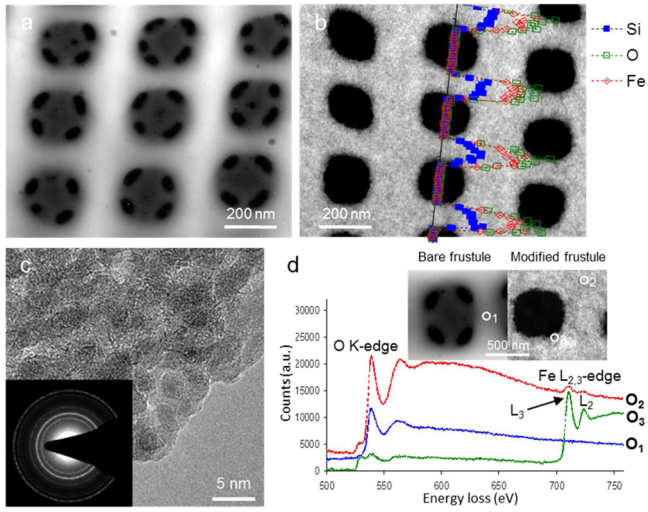

Figure 3. Growth of magnetite NPs onto the periodic structure of frustules. STEM images: (a) bare frustules; (b) magnetite NP-decorated frustules. Inset of b: Corresponding elemental (Fe, O, and Si) profiles along the dashed line. (c) High-resolution TEM image of the magnetite NP-decorated frustule. (d) EELS featuring O K-edge ELNES and Fe L-edges acquired from locations 1, 2, and 3 labeled in the inset dark-field STEM images of the bare and the magnetite NP-decorated frustules.

Si) profiles indicate that a magnetite NP film was uniformly coated on the surface of the biosilica frustule (inset of Figure 3b). The magnetite NPs were crystalline, as indicated by high-resolution TEM imaging and diffraction rings (Figure 3c). The magnetite NPs possessing single magnetic domains[18,19] enabled the decorated frustules, but not the bare frustules, to exhibit superparamagnetism at room temperature (Figure S6). Since these magnetite NPs were extremely small (around 3−8 nm) and tightly packed on the frustule, the heterogeneity among neighboring magnetite NPs was optically negligible in the measured wavelength range.

The distribution of magnetite NPs near the pore edge was assessed by electron energy-loss spectroscopy (EELS), and the spectrum was acquired in a scanning transmission electron microscopy (STEM) mode (Figure 3d). Note in sample location 1 (O1) of the bare frustules that the O K-edge exhibited a slight blue-shift from 532 eV, which is characteristic of amorphous bonding.[20] This edge was split in the presence of magnetite,[21] indicating the additional ordered crystalline bonds of the magnetite NPs. The ratio of this peak-splitting followed the expected trends between the locations labeled as O2 and O3, in accordance with the concentration of amorphously bound oxygen. The increase in plural scattering events is also consistent with the increase in thickness. Since the deposition of magnetite NPs on both the inner and outer surface of the frustule was the same, a trilayered structure was produced.

For purposes of simulation, the magnetite NP-decorated frustule was approximated as a trilayered 2-D photonic crystal slab (magnetite/silica/magnetite) with a thickness of 20, 50, and 20 nm, respectively. The same lattice constant was used with a smaller pore diameter of 160 nm due to the inner pore decoration with magnetite NPs. The calculated TE-like mode photonic band structure shows a "complete" PBG (a/λ, 0.46−

dx.doi.org/10.1021/ph4001185 | ACS Photonics 2014, 1, 477−482

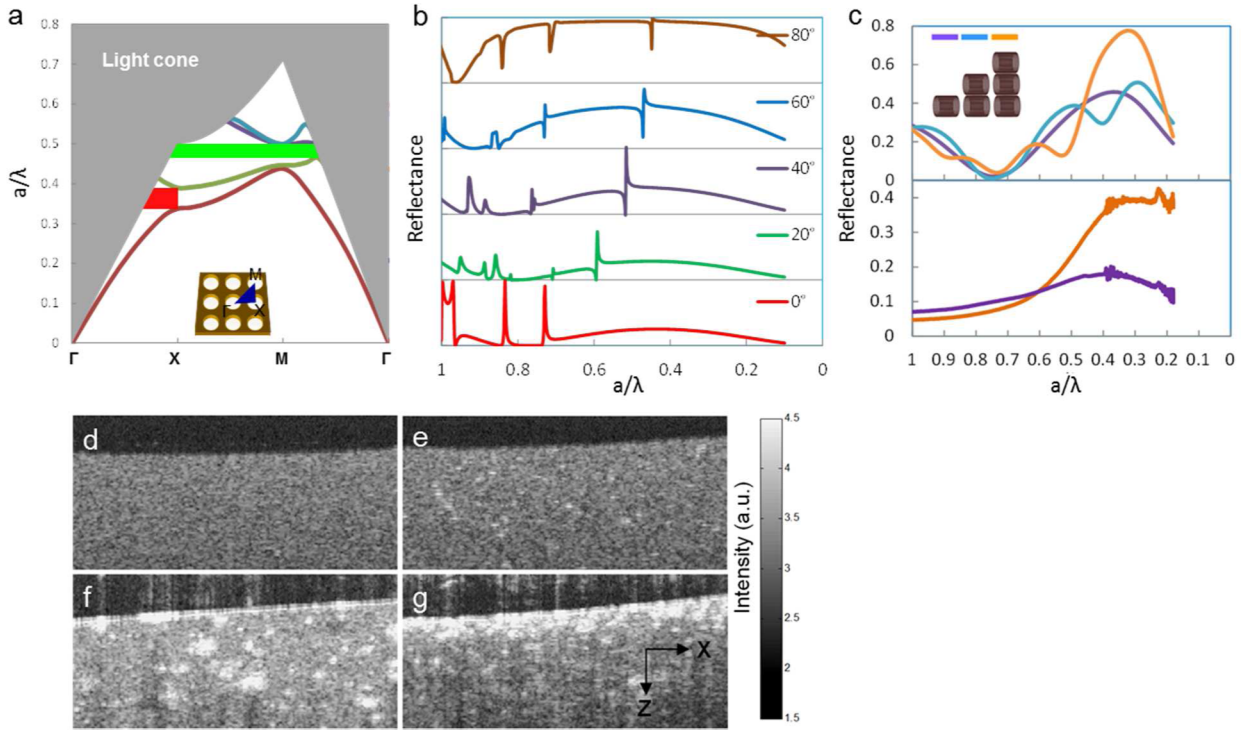

Figure 4. Magnetite NP-decorated frustules are NIR reflective and serve as an efficient contrast-enhancing agent. (a) TE-like mode photonic band structure of the magnetite NP-decorated frustule in air. (b) Calculated angle-resolved reflection spectra of the 2D photonic crystal slab approximated from the magnetite NP-decorated frustule. (c) Top, FDTD-calculated reflectance spectra of mono- (purple), bi- (blue), and tri- (orange) layered magnetite NP-decorated frustule films; bottom, measured reflectance spectra of the films containing nearly monodispersed (purple) or stacked (approximately 2 or 3 layers; orange) magnetite NP-decorated frustules. (d, e, f, and g) 2D (x–z) cross-sectional OCT images of the tissue phantom made of 2 wt % agar, tissue phantoms contained around 5×10^5 mL^{-1} bare frustules, and 5×10^5 mL^{-1} and 2×10^6 mL^{-1} magnetite NP-decorated frustules, respectively. The image size is 1.6×0.65 mm^2 ($x \times z$).

0.50) and a pseudo-PBG (0.33–0.39) under the light line (Figure 4a). No guided modes exist in the gaps; light is forbidden from in-plane propagation and only radiates into the background. The resulting dip in the photonic density of states manifests itself as a reflective peak in the near-infrared. Meanwhile, under off-normal incidence, there were rough coincidences with the reflective peaks shown in the angle-resolved spectra, which were calculated by the scattering matrix method (Figure 4b). At more glancing angles of incidence, the reflective peak expansion from the NIR to the visible range was attributed to the light interference induced by the multilayer film. Based on the combined effects of the PBG and the angle-dependent reflection, the magnetite NP-decorated frustule may produce strong reflection in the NIR range, consistent with its calculated reflectivity spectrum (Figure 4c).

Additionally, stacking magnetite NP-decorated frustules led to stronger NIR reflectance than that of monolayer modified frustules. When we consider the reflection loss related to optical absorption by biosilica and magnetite NPs (Figure S7), our measured reflectivity is in good agreement with the predicted NIR reflectivity from the magnetite NP-decorated frustule films.

In addition, our result shows that magnetite NP-decorated frustules suspended in water are able to selectively reflect NIR light with angular independence (Figure S8). Thus, magnetite NP-decorated frustules serve as "physically brilliant dyes", superior to the conventional dye molecules or pigments that rely on wavelength-selective light absorption and random scattering.

To demonstrate that the magnetite NP-decorated frustules are efficient NIR contrast agents, we imaged the tissue phantoms (2 wt % agar gel) containing the bare frustules or magnetite NP-decorated frustules using an optical coherence tomography (OCT) system at 1310 nm. The schematic of the OCT system is shown in Figure S9.[22,23] In the homogeneous scattering tissue phantom (Figure 4d), the bare frustules demonstrated a relatively low OCT contrast (Figure 4e, generated by backscattered NIR light) no matter whether a low does or a high dose was used. In comparison, the magnetite NP-decorated frustules exhibited a much higher OCT contrast (Figure 4f), which was further enhanced using a high dose of magnetite NP-decorated frustules (Figure 4g). Moreover, a reconstructed 3-D OCT image further indicates that the magnetite NP-decorated frustules are effective OCT contrast agents in tissue phantoms (Figure S10).

In summary, our findings suggest that the diatom *Pinnularia* sp. frustule combines short-range periodicity and long-range isotropy for the wavelength-selective and angle-independent reflection of light. The frustules decorated with high-efficiency refractive index materials exhibit PBG-associated reflection near equally at arbitrary incidence. The significant improvement of the NIR contrast using the magnetite NP-decorated frustules demonstrated by the OCT imaging unveils the potential of these naturally patterned unique structures as photonic crystals for technological applications.

METHODS

Maine diatoms of *Pinnularia* sp. were grown in flask culture for 30 days with an initial silica concentration of 0.5 mmol L^{-1}.

dx.doi.org/10.1021/ph4001185 | *ACS Photonics* 2014, 1, 477–482

The harvested diatoms were treated with hydrogen peroxide for frustule isolation. The frustules were decorated with magnetite NPs through a solvothermal reaction performed at 185 °C for 12 h in a Teflon-lined autoclave. The precursors included 30 mg of frustules, 0.02 mmol of iron(III) acetylacetonate, and 2 mL of oleic acid in 15 mL of ethanol. The dielectric symmetries of the bare or decorated frustules were approximated by morphological and compositional profile (STEM- energy dispersive X-ray spectroscopy and STEM-EELS) analysis. By averaging the measured symmetric parameters of the pore arrays on 20 randomly selected frustules, the structural parameters are approximated as follows: the bare frustules (n_{SiO2} = 1.48), lattice constant a = 325 ± 25 nm, pore diameter d = 200 ± 12 nm, slab thickness h = 50 nm; the magnetite NP-decorated frustules (n_{Fe3O4} =2.42), a = 325 ± 30 nm, d = 160 ± 15 nm. The thickness of the magnetite coating on the frustules was estimated as 20 nm based on the measurement that the pore diameter decreases from 200 to 160 nm after coating magnetite NPs. Thus, the magnetite NP-decorated frustules have a sandwich structure, and the slab thickness of the magnetite, silica, and magnetite is 20, 50, and 20 nm, respectively.

The structural parameters used for all of the numerical simulations are as follows: for the bare frustules, we used a lattice constant of a = 325 nm, a pore diameter of d = 200 nm, and a slab thickness of h = 50 nm, n_{SiO2} = 1.48. For the magnetite NP-decorated frustules, we used a lattice constant of a = 325 nm, a pore diameter of d = 160 nm, and a slab thickness (sandwich structure of magnetite/silica/magnetite) of 20 nm/50 nm/20 nm, n_{SiO2} = 1.48, n_{Fe3O4} = 2.42. The photonic band structures of the bare frustules and magnetite NP-decorated frustules in transverse modes (TE-like) were calculated by a plane wave expansion method. A 2-D photonic crystal slab was centered in the vertical dimension of the supercell and surrounded by air, all of which are infinitely extended in the x and y directions and repeated in the z direction. It is important that the air space between the slabs in the z direction is sufficient so that coupling of the guided modes between the slabs is minimized. Their solutions become part of the background continuum of modes that is shown by the shaded region of the band structure. For FDTD simulations, a numerical model was set up under Meep, a free FDTD simulation software package, to calculate the reflection spectrum of the bare frustules and magnetite NP-decorated frustules. The size of the 3-D computational domain enclosing the frustules is specified as $50a \times 60a \times 10a$, where a = 325 nm.

For optical measurements, stacked frustule films with different thicknesses were formed by depositing different amounts of the bare or magnetite NP-decorated frustules in a limited area. The reflectivity spectra were measured using a spectrophotometer attached with a UV−vis−NIR integrating sphere. For the OCT imaging test, the bare or magnetite NP-decorated frustules were also dispersed into 2 wt % agar gel at 85 °C. After cooling to near room temperature, the resulting tissue phantoms were scanned using the OCT system shown in Figure S9.

■ ASSOCIATED CONTENT

Supporting Information

SEM images and AFM profiles of frustule pore structures, TEM images of magnetite NPs, optical and MFM images of magnetite NP-decorated frustules, a schematic of our OCT system, and a 3-D OCT image of the tissue phantom containing magnetite NP-decorated frustules are presented. This material is available free of charge via the Internet at http://pubs.acs.org.

■ AUTHOR INFORMATION

Corresponding Author

*E-mail: jiaoj@pdx.edu.

Notes

The authors declare no competing financial interest.

■ ACKNOWLEDGMENTS

We thank A. Besser for the EELS spectrum acquisition. This work was supported in part by grants from NSF (J.J.), ONAMI (J.J.), and SNNI-AFRL (G.R. and J.J.).

■ REFERENCES

(1) Kinoshita, S.; Yoshioka, S.; Miyazaki, J. Physics of structural colors. *Rep. Prog. Phys.* **2008**, *71*, 076401.
(2) Vukusic, P.; Sambles, J. R. Photonic structures in biology. *Nature* **2003**, *424*, 852−855.
(3) Round, F. E., Craford, R. M.; Man, D. G. *The Diatoms*; Cambridge University Press, 1990.
(4) Sumper, M.; Brunner, E. Learning from diatoms: nature's tools for the production of nanostructured silica. *Adv. Funct. Mater.* **2006**, *16*, 17−26.
(5) Hamm, C. E.; Merkel, R.; Springer, O.; Jurkojc, P.; Maier, C.; Prechtel, K.; Smetacek, V. Architecture and material properties of diatom shells provide effective mechanical protection. *Nature* **2003**, *421*, 841−843.
(6) Furukawa, T.; Watanabe, M.; Shihira-Ishikawa, I. Green- and blue-light-mediated chloroplast migration in the centric diatom *Pleurosira laevis*. *Protoplasma* **1998**, *203*, 214−220.
(7) Joannopoulos, J. D.; Johnson, S. G.; Winn, J. N.; Meade, R. D. *Photonic Crystals: Molding the Flow of Light* (2d ed.); Princeton University Press, 2008.
(8) Johnson, S. G.; Joannopoulos, J. D. Block-iterative frequency-domain methods for Maxwell's equations in a planewave basis. *Opt. Express* **2001**, *8*, 173−190.
(9) Fuhrmann, T.; Landwehr, S.; El Rharbi-Kucki, M.; Sumper, M. Diatoms as living photonic crystals. *Appl. Phys. B: Laser Opt.* **2004**, *78*, 257−260.
(10) Jeffryes, C.; Solanki, R.; Rangineni, Y.; Wang, W.; Chang, C.; Rorrer, G. L. Electroluminescence and photoluminescence from nanostructured diatom frustules containing metabolically inserted germanium. *Adv. Mater.* **2008**, *20*, 2633−2637.
(11) Oskooi, A. F.; Roundy, D.; Ibanescu, M.; Bermel, P.; Joannopoulos, J. D.; Johnson, S. G. MEEP: A flexible free-software package for electromagnetic simulations by the FDTD method. *Comput. Phys. Commun.* **2010**, *181*, 687−702.
(12) Johnson, S. G.; Fan, S.; Villeneuve, P. R.; Joannopoulos, J. D.; Kolodziejski, L. A. Guided modes in photonic crystal slabs. *Phys. Rev. B* **1999**, *60*, 5751−5758.
(13) Whittaker, D. M.; Culshaw, I. S. Scattering-matrix treatment of patterned multilayer photonic structures. *Phys. Rev. B* **1999**, *60*, 2610−2618.
(14) Noh, H.; Liew, S. F.; Saranathan, V.; Mochrie, S. G. J.; Prum, R. O.; Dufresne, E. R.; Cao, H. How noniridescent colors are generated by quasi-ordered structures of bird feathers. *Adv. Mater.* **2010**, *22*, 2871−2880.
(15) Ekelund, N. G. A.Effects of UV-B radiation on growth and motility of four phytoplankton species. *Physiol. Plant.* **1991**, *78*, 590−594.
(16) Lin, S. Y.; Fleming, J. G.; Hetherington, D. L.; Smith, B. K.; Biswas, R.; Ho, K. M.; Sigalas, M. M.; Zubrzycki, W.; Kurtz, S. R.; Bur, J. A three-dimensional photonic crystal operating at infrared wavelengths. *Nature* **1998**, *398*, 251−253.

(17) de Stefano, L.; Maddalena, P.; Moretti, L.; Rea, I.; Rendina, I.; de Tommasi, E.; Mocella, V.; de Stefano, M. Nano-biosilica from marine diatoms: A brand new material for photonic applications. *Superlattices Microstruct.* **2008**, *46*, 84−89.
(18) Chueh, Y. L.; Lai, L. W.; Liang, J. Q.; Chou, L. Z.; Wang, Z. L. Systematic study of the growth of aligned arrays of α-Fe_2O_3 and Fe_3O_4 nanowires by a vapor-solid process. *Adv. Funct. Mater.* **2006**, *16*, 2243−2251.
(19) Iida, H.; Takayanagi, K.; Nakanishi, T.; Osaka, T. Synthesis of Fe_3O_4 nanoparticles with various sizes and magnetic properties by controlled hydrolysis. *J. Colloid Interface Sci.* **2007**, *314*, 274−280.
(20) Lichtenberger, O.; Neumann, D. A study of Si-L and O-K KLNES in plant material: SiO_2, Ca- and Zn-silicate in Minuartia. *J. Microsc.* **1996**, *183*, 45−52.
(21) Colliex, C.; Manoubi, T.; Ortiz, C. Electron-energy-loss-spectroscopy near-edge fine structures in the iron-oxygen system. *Phys. Rev. B* **1991**, *44*, 11402−11411.
(22) Wang, R. K.; Jacques, S. L.; Ma, Z.; Hurst, S.; Hanson, S. R.; Gruber, A. Three dimensional optical angiography. *Opt. Express* **2007**, *15*, 4083−4097.
(23) Wang, R. K.; Hurst, S. Mapping of cerebro-vascular blood perfusion in mice with skin and skull intact by optical micro-angiography at 1.3 μm wavelength. *Opt. Express* **2007**, *15*, 11402−11412.